CHALMERS
UNIVERSITY OF TECHNOLOGY

Noise Performance of Single-Mode VCSELs: Dependence on Current Confinement and Optical Loss

Noise Performance of Single-Mode VCSELs: Dependence on Current Confinement and Optical Loss

Ewa Simpanen, *Member, IEEE, Student Member, OSA*, Johan S. Gustavsson, Pierluigi Debernardi, Wayne V. Sorin, *Fellow, IEEE*, Sagi Mathai, *Senior Member, IEEE*, Michael R. Tan, and Anders Larsson, *Fellow, IEEE, Fellow, OSA*

***Abstract*—We investigate the intensity and phase noise properties of GaAs-based 1060 nm oxide-confined single-mode vertical-cavity surface-emitting lasers (VCSELs) and their dependence on slope efficiency and current spreading, parameters that control the achievable output power. We find strong dependence of the linewidth on slope efficiency because it affects the optical resonator loss and therefore the spontaneous emission rate and the photon density. Likewise, we find strong dependence of the relative intensity noise on the slope efficiency since the optical resonator loss controls the photon lifetime, and therefore the damping of the relaxation oscillations. There is no noticeable dependence on transverse current confinement and current spreading. We measure linewidths as small as 6 MHz which we attribute to a small linewidth enhancement factor. This assumption is supported by calculations of the linewidth enhancement factor from optical resonator and optical gain simulations. The dependencies of noise on design parameters are general and therefore valid for single-mode VCSELs at other wavelengths and in other material systems.**

***Index Terms*—Linewidth, noise, RIN, single-mode, vertical-cavity surface-emitting lasers.**

I. Introduction

THE vertical-cavity surface-emitting laser (VCSEL) is the preferred light source for an increasing number of applications, ranging from datacom and optical interconnects [1] to 3D sensing [2] and LIDAR [3]. In applications requiring spectral purity or coherence, single-mode (SM) VCSELs are needed. This includes e.g. extended reach optical interconnects using single-mode fiber (SMF) [4], gas sensing based on tunable diode laser absorption spectroscopy [5], laser mouse sensors [6], and VCSEL-based atomic clocks [7]. Here the intensity and/or phase noise properties of the VCSEL are of importance since they limit system performance.

Manuscript received January 22, 2020. This work was supported by the Hewlett Packard Enterprise Innovation Research Program, the Swedish Foundation for Strategic Research under Grant SE13-0014, and the Swedish Research Council under Grant 2016-06077.

E. Simpanen, J. S. Gustavsson, and A. Larsson are with Photonics Laboratory, Department of Microtechnology and Nanoscience, Chalmers University of Technology, SE 41296 Gothenburg, Sweden (e-mail: ewa.simpanen@chalmers.se; johan.gustavsson@chalmers.se; anders.larsson@chalmers.se).

P. Debernardi is with Consiglio Nazionale delle Ricerche, Istituto di Elettronica e di Ingegneria delle Telecomunicazioni, 10129 Turin, Italy (e-mail: pierluigi.debernardi@ieiit.cnr.it).

W. V. Sorin, S. Mathai, and M. Tan are with Hewlett Packard Enterprise, 1501 Page Mill Road, Palo Alto, CA 94304-1123, USA (e-mail: wayne.sorin@hpe.com; sagi.mathai@hpe.com; mike.tan@hpe.com).

Previous work has shown that properly designed SM-VCSELs can have intensity noise, quantified as the relative intensity noise (RIN), approaching the shot noise level at high current and output power [4]. This is in contrast to multimode VCSELs where the low frequency RIN is enhanced by mode competition [8]. The phase noise of SM-VCSELs, quantified as the linewidth, varies greatly depending on design. Minimum linewidths for GaAs-based SM-VCSELs range from a few MHz to more than 100 MHz [9], [10].

In applications requiring SM-VCSELs, it is generally desirable to reach high output power at a low current. This can be achieved with a VCSEL with high slope efficiency. However, the increased optical resonator loss translates to an increased threshold gain and threshold carrier density and a reduced photon density in the active region. It is therefore of interest to understand to what extent the slope efficiency (or equivalently the optical resonator loss) affects the intensity and phase noise.

Output power is also limited by self-heating which, for a small-aperture high-resistance SM-VCSEL, is caused primarily by Joule heating. Positioning the oxide aperture of a GaAs-based oxide-confined VCSEL at a relatively large distance above the active region results in current spreading under the aperture [11] that feeds higher order transverse modes. A very small aperture in then needed for sufficient suppression of higher order modes, which leads to high resistance and limited output power. Current spreading can be reduced by positioning the aperture closer to the active region [12]. This allows for larger aperture SM-VCSELs with lower resistance and higher output power. It is well known that spatial effects such as current spreading and spatial hole burning induced carrier diffusion can have large impact on the noise properties of oxide-confined SM-VCSELs [13]. In addition, the randomness of carrier diffusion is known to be a major source of noise in semiconductors [14]. It is therefore also of interest to investigate to what extent current spreading (or equivalently transverse current confinement) may affect the intensity and phase noise.

In this paper we report on the intensity and phase noise properties of 1060 nm GaAs-based oxide-confined SM-VCSELs that differ in terms of optical resonator loss (slope efficiency) and transverse current confinement (current spreading). We find a strong dependence of RIN and linewidth on optical resonator loss while there is no noticeable dependence on current confinement. We measure linewidths as low as 6 MHz and attribute this to a small linewidth enhancement factor.

In Section II, we introduce the VCSEL designs, the technique used to control the slope efficiency, and the basic performance of the VCSELs. Results from RIN and linewidth measurements are presented in Section III and IV, respectively. Section V presents a brief theoretical phase noise analysis to explain the low linewidths measured and the dependence on resonator loss. Conclusions are presented in Section VI.

II. VCSEL Designs and Basic Performance

The 1060 nm GaAs-based oxide-confined VCSELs were fabricated from two all-semiconductor epitaxial designs, differing in the distance between the oxide aperture and the active region. The designs, referred to as D1 and D2, are illustrated in Fig. 1 and presented in detail in [15]. Both designs employ multiple oxide apertures with the thickness of doped material between the primary apertures (used for transverse optical and current confinement and positioned at nodes of the optical field) and the active region being 177 and 19 nm for design D1 and D2, respectively. We therefore expect more current spreading under the apertures in design D1. This was confirmed by spontaneous emission near field imaging. Fig. 2 displays near field images of VCSELs from D1 and D2, both with 2.5 µm diameter primary oxide apertures and biased at 50 µA (well below threshold). The images were recorded by projecting the VCSEL surface on a Spiricon BGP-USB-SP928-OSI CCD camera with Beam Gage software using a 20x microscope objective and a 4x projection lens. With the spontaneous emission mapping the transverse distribution of carriers in the active region, it is clear that design D1 suffers from significant current spreading while moving the apertures closer to the active region (D2) can to a large extent suppress spreading.

The more strongly confined current in design D2 translates to more strongly confined optical gain. Consequently, it was found that the maximum aperture diameter allowing for SM operation with >35 dB suppression of higher order modes is 3.5 µm for design D2, while it is only 2.5 µm for design D1 with less confined current and gain (as indicated in Fig. 1). To compare VCSELs with the same requirement in terms of mode suppression, these are the aperture sizes used in the following RIN and linewidth measurements.

For both designs, we fabricated VCSELs with different slope efficiency. The slope efficiency was controlled by the reflectance of the top-distributed Bragg reflector (DBR) which was set by the thickness of the top layer [16]. The initial optical thickness of this layer was half a wavelength, which creates an anti-phase reflection at the surface that lowers the DBR reflectance. By controlled thinning using dry etching the reflectance was increased, and consequently the slope efficiency reduced. The dependence of the slope efficiency on etch depth, calculated using a 1D effective index model for the optical resonator properties with different above threshold internal quantum efficiencies, is shown in Fig. 3. Through measurements of the slope efficiency with increasing etch depth, we found a minimum slope efficiency of ~0.5 W/A at an etch depth of 70-80 nm (where the thickness of the top layer is close to a quarter wavelength) which, according to Fig. 3, suggests an internal quantum efficiency of ~90%. We assume this to be the same for both designs since the above threshold internal quantum efficiency should not be affected by current spreading [11]. For the proceeding measurements we chose VCSELs with slope efficiencies of 0.52 and 0.75 W/A from both designs. This corresponds to etch depths of ~63 and ~27 nm, respectively (Fig. 3).

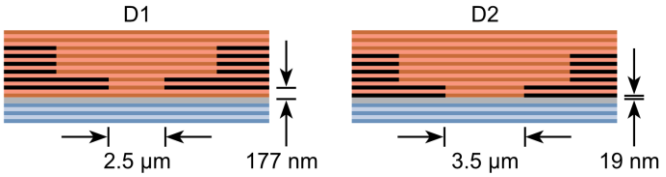

Fig. 1. Cross-sectional schematics of the two designs, D1 and D2, illustrating the difference in position of the multiple oxide apertures (2 primary and 4 secondary) relative to the active region, as well as the difference in aperture diameter for VCSELs with similar suppression of higher order modes.

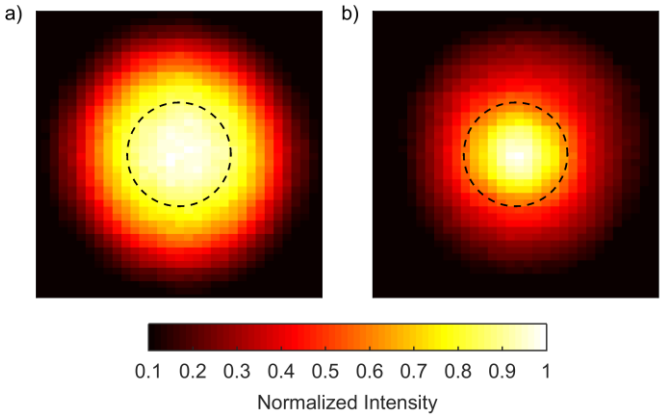

Fig. 2. Normalized near-field intensity images for VCSELs with aperture diameters of 2.5 µm (dashed circle) biased at 50 µA, from a) D1 and b) D2.

The measured output power and voltage vs. current for the D1 VCSELs with 2.5 µm aperture and the D2 VCSELs with 3.5 µm aperture is shown in Fig. 4. Optical power was recorded using a calibrated large-area Ge-photodiode. All

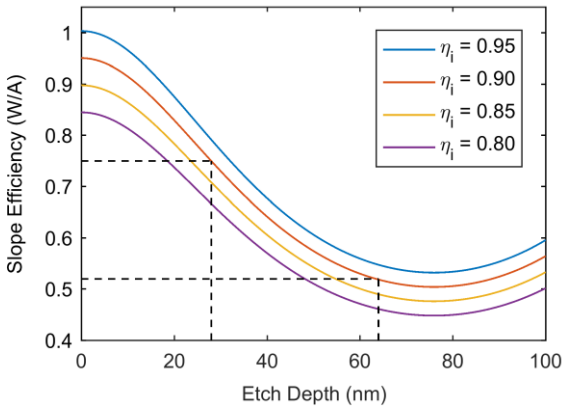

Fig. 3. Calculated dependence of slope efficiency on etch depth for different above threshold internal quantum efficiencies. The dependence applies to both designs. At etch depth = 0 nm, the optical thickness of the top layer is half a wavelength. At etch depth = 76 nm it is a quarter wavelength. The dashed lines indicate the etch depths for the 0.52 and 0.75 W/A slope efficiency VCSELs with ~90% internal quantum efficiency.

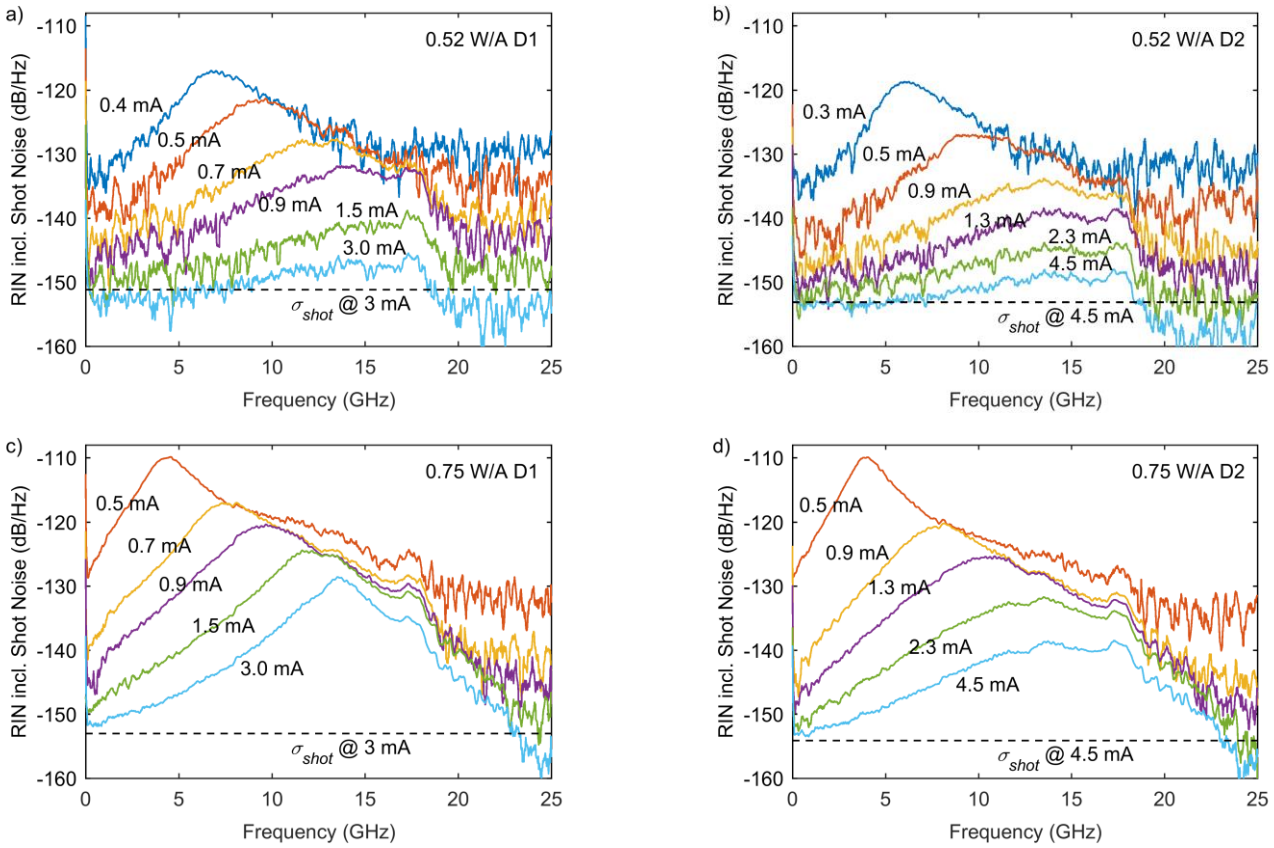

Fig. 6. RIN including shot noise for low slope efficiency VCSELs from design a) D1 and b) D2, and for high slope efficiency VCSELs from design c) D1 and d) D2, at indicated bias currents.

measurements were performed at 25°C. Clearly, the higher slope efficiency enables higher output power despite a larger threshold current. Also, the larger aperture D2 VCSELs deliver a higher maximum power because of delayed thermal rollover due to the lower resistance. At half the thermal rollover current, the differential resistance is ~570 and ~290 Ω for D1 and D2, respectively. Notable is also the fact that the threshold currents for the D2 VCSELs are smaller than for the D1 VCSELs, despite the larger oxide apertures. This is a result of the stronger transverse current confinement.

Emission spectra were recorded with an ANDO AQ6317 optical spectrum analyzer and an OM4 fiber butt-coupled to the VCSELs. Fig. 5 shows spectra when the VCSELs were biased at a current for half the maximum output power. The suppression of higher order transverse modes is similar and >35 dB in all cases.

III. RIN Measurements

RIN, which quantifies the optical power fluctuation relative the average optical power, and its dependence on frequency, was calculated from the measured electrical noise power spectral densities according to [17]:

$$RIN(f) = \frac{\sigma_{tot}(f) - \sigma_{th}(f)}{I_0^2 \cdot R_L} - \sigma_{shot}\,, \tag{1}$$

where σ_{tot} denotes the total system noise power with the VCSEL turned on. It was measured with a 50 GHz Agilent PXA N9030A signal analyzer, using a 25 GHz New Focus 1414 MM photodetector to receive the VCSEL output power, and a 25 GHz bandwidth, 27 dB gain low-noise amplifier (SHF 115AP) to bring the signal power above the noise floor of the signal analyzer. The spectrum of the thermal noise power σ_{th} was recorded with the VCSEL turned off, before a sequence of spectra were captured for the total noise power with the VCSEL biased at different currents. At each bias current, the detector DC photocurrent I_0 was measured to calculate the corresponding shot noise power σ_{shot} ($=2q/I_0$), and together with the detector load resistance RL, the average power. The frequency response of the amplifier was accounted for by measuring its response with a Rohde & Schwarz ZVA vector network analyzer and the detector output was used as the common reference point for all noise powers.

With SM-VCSELs being sensitive to optical feedback [18], the VCSEL optical output was coupled to the input single-mode fiber (SMF) of a Thorlabs IO-H-1064B-APC optical isolator via an anti-reflection coated lens package. The beam was magnified to match the mode-field diameter of the SMF, and the coupling efficiency was ~75%. The fiber was also tilted at a small angle to avoid feedback from the fiber end face. The output SMF of the optical isolator was connected to the photodetector.

The noise spectra in Fig. 6 show the sum of RIN and shot noise for bias currents from just above threshold to ~75% of the thermal rollover current. As expected, the intensity noise

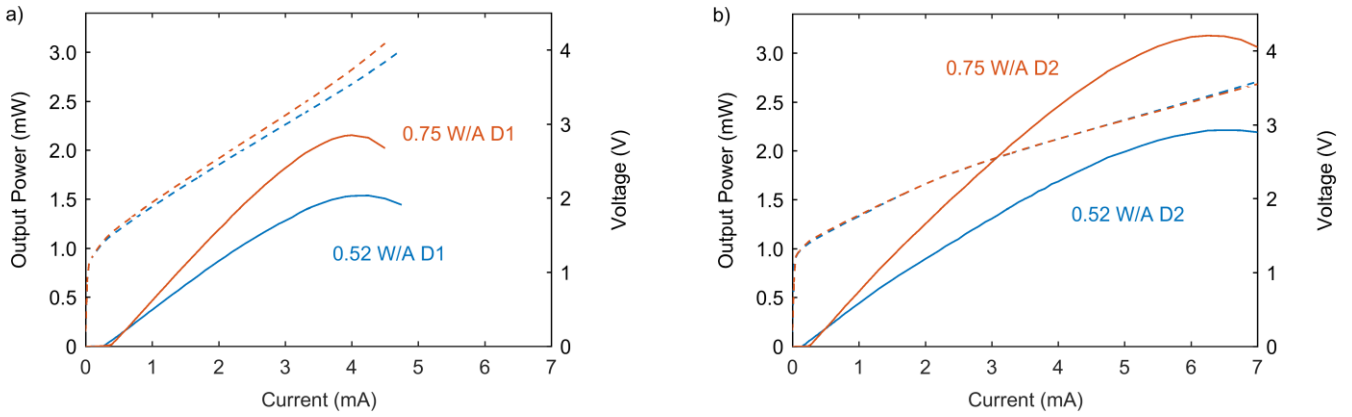

Fig. 4. Optical output power (solid) and voltage (dashed) vs. current for VCSELs with slope efficiencies of 0.52 W/A (blue) and 0.75 W/A (red), from design a) D1 with weaker, and b) D2 with stronger transverse current confinement.

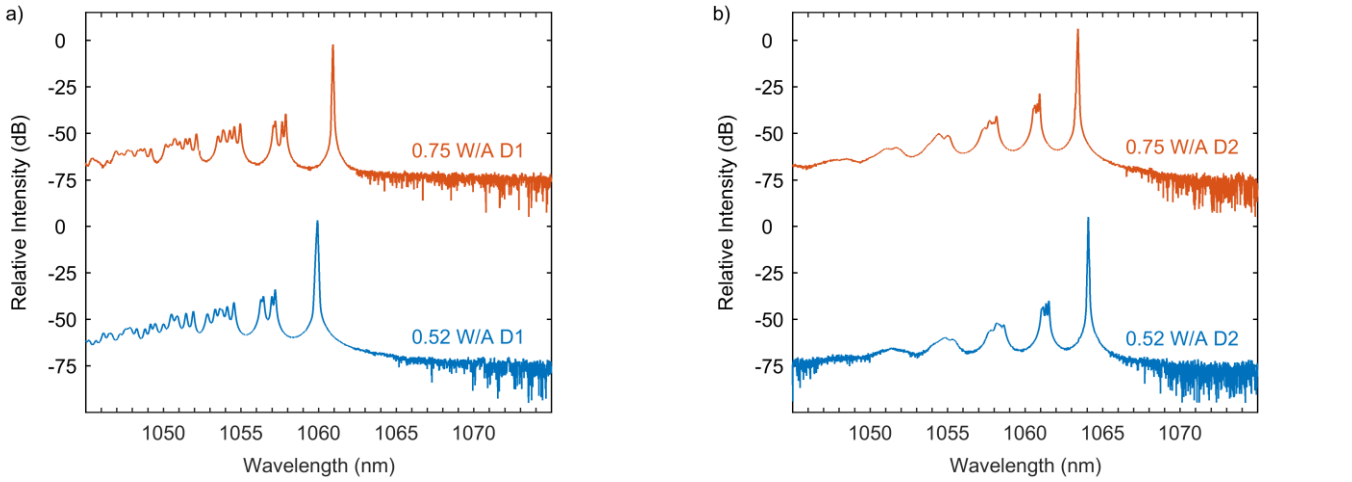

Fig. 5. Spectra for VCSELs with slope efficiencies of 0.52 W/A (blue) and 0.75 W/A (red), from a) D1 biased at 2 mA and b) D2 at 3 mA.

peaks at the relaxation frequency and both the relaxation frequency and the damping rate increases with current. A clear difference is seen between the low and high slope efficiency VCSELs, with the intensity noise of the low slope efficiency VCSELs approaching the shot noise level (indicated by dashed lines in Fig. 6 at the highest bias current) at high currents. The intensity noise of the high slope efficiency VCSELs is considerably higher due to the smaller photon lifetime and the lower photon density in the active region, which leads reduced damping of the relaxation oscillations. The average intensity noise (RIN + shot noise), plotted as a function of output power in Fig. 7, shows a ~10 dB higher noise level at high powers for the high slope efficiency VCSELs. The dependence of intensity noise on optical resonator loss is therefore strong. In contrast, there is no noticeable dependence of intensity noise on transverse current confinement.

IV. Linewidth Measurements

Linewidths were measured using a Toptica FPI 100-1064-3V0 scanning Fabry-Perot interferometer (FPI) with a finesse >625 and a free spectral range of 1 GHz, hence a resolution of ~1.6 MHz. The same techniques used for preventing optical feedback in the RIN measurements were used for the linewidth measurements. Additional precautions were taken to eliminate additional noise from mechanical vibrations, thermal fluctuations, and connector loss. A low noise Yokogawa 7651 DC current source was used to bias the VCSELs. A Miniscan 102 scan generator with a scan voltage of 25 V and a scan frequency of ~45 Hz was used to sweep the FPI over more than a free spectral range to be able to convert scan voltage to frequency. The output from the photodiode amplifier of the FPI was connected to a Rigol DS4014E digital oscilloscope to record the scan trace. Linewidths were extracted using Lorentzian curve fitting.

Linewidths plotted vs. the inverse of the optical output power, which enables the linewidth-power product to be determined, are shown in Fig. 8a. Fig. 8b shows an example of a scan trace with a Lorentzian fit (the 0.75 W/A D1 VCSEL biased at 0.8 mA). As for RIN, there is a clear difference between high and low slope efficiency VCSELs but no clear dependence on transverse current confinement. The higher resonator loss for the high slope efficiency VCSELs results in higher threshold gain and threshold carrier density, which leads to increased spontaneous emission and hence larger linewidths. The linewidth-power product for the low slope efficiency VCSELs is ~0.5 MHz·mW while it is ~1.7 MHz·mW for the high slope efficiency VCSELs. The

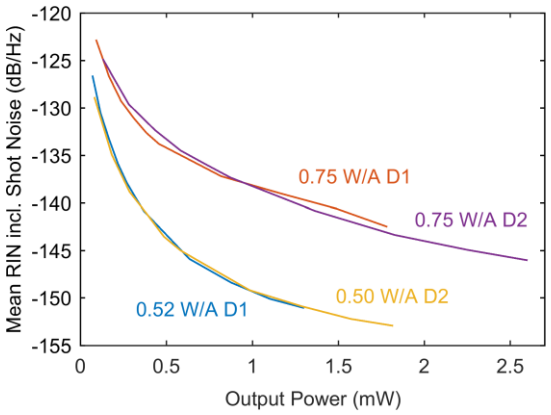

Fig. 7. RIN including shot noise averaged over frequencies up to 25 GHz, vs. VCSEL output power.

minimum linewidth is ~6 MHz, which is relatively small in comparison with linewidths of GaAs-based oxide-confined VCSELs reported in the literature [9], [10]. At higher optical power, the linewidth no longer follows the inverse optical power dependence and a slight broadening of the linewidth was observed. This could be caused by strong self-heating at high currents, which leads to significantly higher threshold carrier density and spontaneous emission rate. According to Fig. 8, the D1 VCSELs have a lower residual linewidth (extrapolation to zero inverse optical power). This could possibly be related to the higher series resistance generating a lower thermal noise current.

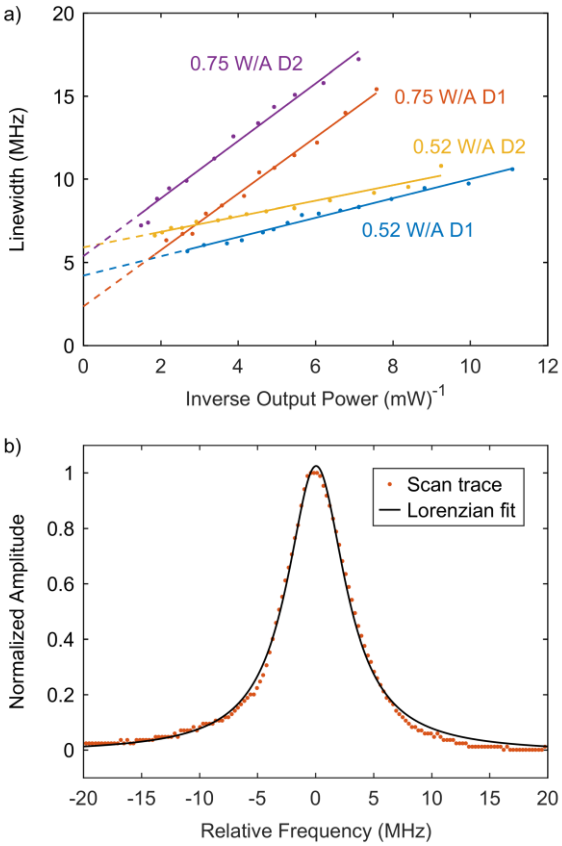

Fig. 8. a) Linewidth vs. inverse output power for each of the four VCSELs. b) Scan trace and Lorentzian fit with a D2 0.52 W/A VCSEL biased at 1.1 mA, thus providing an output power of ~0.49 mW.

V. Analysis

With the assumption of spontaneous emission into the lasing mode being the source of noise, the linewidth $\Delta\nu$ of the lasing mode can be calculated from the modified Schawlow-Townes formula [19]:

$$(\Delta\nu)_{ST} = \frac{R_{sp}}{4\pi N_p}, \tag{2}$$

where R_{sp} is the rate of spontaneously emitted photons into the mode and N_p is the photon number in the mode. When also accounting for the amplitude-phase coupling that broadens the linewidth of semiconductor lasers, through the α-parameter (or linewidth enhancement factor) [20], (2) becomes:

$$\Delta\nu = \frac{R_{sp}}{4\pi N_p}\cdot\left(1+\alpha^2\right). \tag{3}$$

Expressed in terms of VCSEL parameters, (3) is converted to [21]:

$$\Delta\nu = \frac{\left(\Gamma v_g g_{th}\right)^2 \eta_0}{4\pi P_0} n_{sp}\frac{hc}{\lambda}\cdot\left(1+\alpha^2\right). \tag{4}$$

This equation contains the optical confinement factor Γ, the group velocity v_g, the threshold gain g_{th}, the optical outcoupling efficiency η_0, the optical output power P_0, the population inversion factor n_{sp}, and the photon energy hc/λ. For the group velocity we use a value of $8.3\cdot10^7$ m/s [22]. The optical outcoupling efficiency is calculated from the various optical loss rates in the VCSEL resonator, or from the slope efficiency (SE), internal quantum efficiency η_i, and photon energy:

$$\eta_0 = \frac{\alpha_T}{\alpha_T+\alpha_B+\alpha_i} = \frac{SE}{\eta_i}\cdot\frac{q\lambda}{hc}, \tag{5}$$

where α_T and α_B are the loss rates through the top and bottom DBR and α_i is the internal loss rate due to free carrier absorption. The population inversion factor is calculated from the quasi-Fermi level separation ΔE_F at the carrier density needed to reach the threshold gain:

$$n_{sp} = \frac{1}{1-\exp\left(\left(hc/\lambda-\Delta E_F\right)/kT\right)}. \tag{6}$$

For calculations of the optical confinement factor, the threshold gain, and the outcoupling efficiency, we use the same 1D effective index model that was used to calculate the dependence of slope efficiency on etch depth in Fig. 2. The calculated dependence of threshold gain on etch depth is shown in Fig. 9.

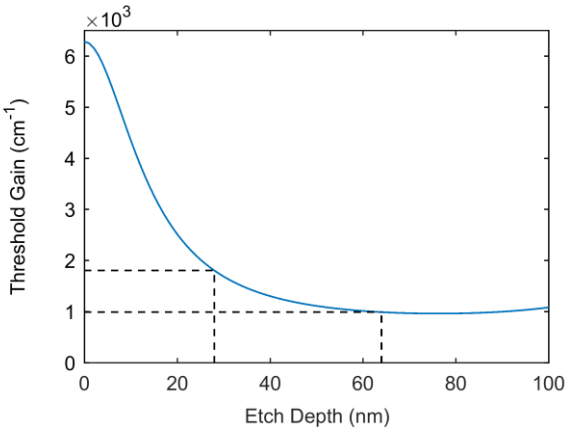

Fig. 9. Calculated dependence of threshold gain on etch depth. The dashed lines show the threshold gains for the different slope efficiency VCSELs, from the etch depths in Fig. 3.

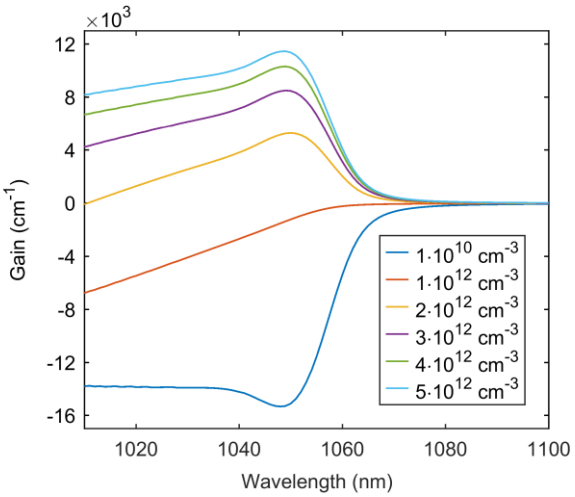

Fig. 10. Calculated gain spectra at different carrier densities in the QWs.

To calculate the quasi-Fermi level separation, and therefore the population inversion factor, we used an optical gain model where the band structure is calculated using a 4x4 $k{\cdot}p$ model and a non-Markovian broadening of the transitions is used [23]. The In-concentration in the strained InGaAs quantum wells (QWs), separated by partly strain-compensating GaAsP barriers, was fine-tuned to set the spontaneous emission wavelength from the gain model at 1050 nm at low carrier density. This is the measured photoluminescence wavelength from the QWs under low excitation conditions. The gain spectrum was subsequently calculated at different excess carrier densities and the result is shown in Fig. 10.

The gain model was subsequently used to calculate the threshold carrier densities for the different slope efficiency VCSELs from the threshold gains in Fig. 9, as illustrated in Fig. 11a. The quasi-Fermi levels were calculated from the threshold carrier densities (Fig. 11b).

The parameters in (4) and the Schawlow-Townes linewidth-power products calculated from those parameters are listed in Table I for the 0.52 and 0.75 W/A slope efficiency VCSELs.

From the calculated Schawlow-Townes linewidth-power products and the measured linewidth-power products (Section IV), we estimate the α-parameter to be -0.2 to -0.5 using (4). This is in fair agreement with the value predicted by the optical gain model, which is approximately -1 (Fig. 11c). The small linewidths and linewidth-power products are clearly the result of a small α-parameter.

The higher outcoupling efficiency, which reduces the photon density in the active region, and the higher threshold carrier density, which increases the spontaneous emission rate, explains the larger linewidths and linewidth-power products for the higher slope efficiency VCSELs (Equation (2)).

With spontaneous emission being the fundamental source of noise for both intensity and phase noise, they are correlated. RIN is expected to be directly proportional to the linewidth, but also frequency dependent due to the restoring force on the carrier density causing relaxation oscillations [24]:

$$\frac{RIN}{\Delta f} \approx (\Delta\nu)_{ST} \cdot \frac{Af^2 + B}{\left(f^2 - f_r^2\right)^2 + \left(\gamma/2\pi\right)^2}, \tag{7}$$

where f_r is the frequency and γ is the damping rate of the relaxation oscillations. A comparison of the linewidths for the high and low slope efficiency VCSELs (Section IV), suggests a ~5 dB higher RIN level for the high slope efficiency

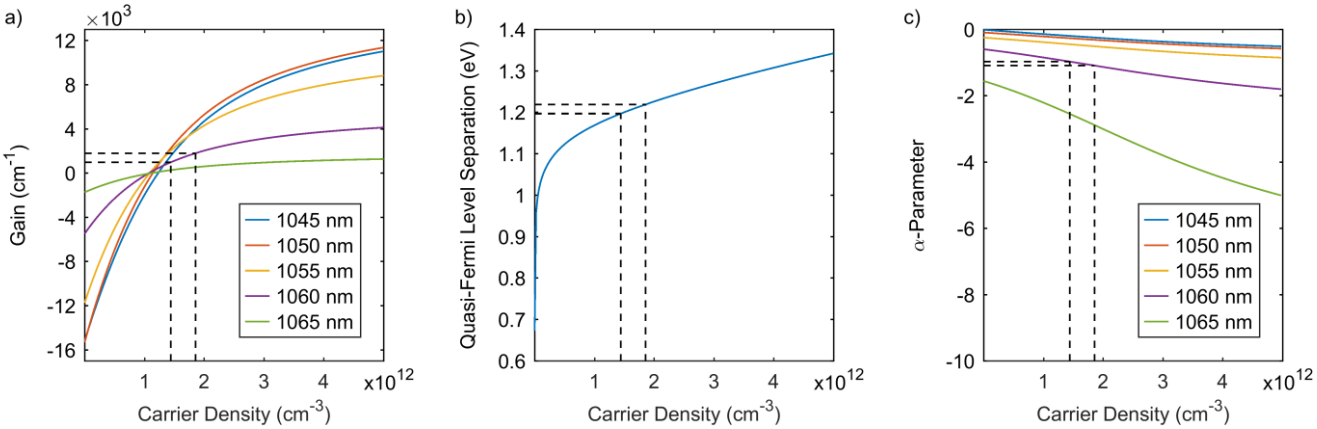

Fig. 11. a) Dependence of optical gain on carrier density at different wavelengths. b) Dependence of quasi-Fermi level separation on carrier density. c) Dependence of the α-parameter on carrier density at different wavelengths. The dashed lines show how carrier densities are obtained from the threshold gains (a) and how the quasi-Fermi level separations (b) and α-parameters (c) are obtained from the carrier densities, for the different slope efficiency VCSELs.

TABLE I
SUMMARY OF VCSEL PARAMETERS CALCULATED FROM THE OPTICAL 1D EFFECTIVE INDEX MODEL AND THE GAIN MODEL.

Symbol	Quantity	Low SE VCSEL	High SE VCSEL
SE	Slope efficiency (W/A)	0.52	0.75
g_{th}	Threshold gain (cm^{-1})	990	1800
Γ	Optical confinement factor	0.0245	0.0244
η_0	Outcoupling efficiency	0.494	0.713
n_{th}	Threshold carrier density (cm^{-2})	$1.44 \cdot 10^{12}$	$1.85 \cdot 10^{12}$
ΔE_F	Quasi-Fermi level separation (eV)	1.197	1.219
n_{sp}	Population inversion factor	1.532	1.174
$(\Delta\nu \cdot P_0)_{ST}$	Schawlow-Townes linewidth-power product (MHz·mW)	0.46	1.66

VCSEL. The much higher RIN measured is therefore primarily a consequence of the less damped oscillations, which enhances RIN at the relaxation oscillation frequency. The reduced damping is a consequence of the reduced photon lifetime in the higher loss resonator [16].

For a more quantitative analysis of the impact of spontaneous emission rate (R_{sp}) and photon density (N_p) on linewidth, we have calculated these quantities using [21]:

$$R_{sp} = \frac{\Gamma v_g g_{th} n_{sp}}{V}, \quad (8) \quad \text{and} \quad N_p = \frac{\Gamma \lambda}{v_g \alpha_T hcV} \cdot P_0, \quad (9)$$

where V is the active region volume. A comparison of high and low slope efficiency VCSELs from design D2 reveals that the ~4 times larger linewidth for the former is caused by a 1.4 times higher spontaneous emission rate as a result of the higher threshold gain and therefore higher threshold carrier density, and a 0.4 times lower photon density as a result of the higher loss rate through the top-DBR. The 0.8 times smaller population inversion factor (stronger inversion) is outweighed by the 1.8 times larger threshold gain (Equation (4) and Table I). The slightly larger α-parameter (Fig. 11c) contributes only marginally to the larger linewidth.

For the impact of damping on RIN, we have used small signal modulations response (S21) data for the high and low slope efficiency D2 VCSELs to extract the D-factor, K-factor, and damping offset (γ_0) through fitting of a transfer function representing the intrinsic and parasitic response [16]. For the high slope efficiency VCSEL we have D = 13.0 GHz/mA$^{1/2}$, K = 0.15 ns, and γ_0 = 14 ns^{-1}, while the corresponding numbers for the low slope efficiency VCSEL are 16.2 GHz/mA$^{1/2}$, 0.23 ns, and 16 ns^{-1}. This enables us to compute the resonance frequency and the damping rate at a given output power or current. At 1 mW output power, the resonance frequency and the damping rate for the high slope efficiency VCSEL are 14.9 GHz and 47 ns^{-1}, respectively, while the corresponding numbers for the low slope efficiency VCSEL are 23.4 GHz and 142 ns^{-1}. With RIN at the resonance frequency being proportional to the frequency squared and the inverse of the damping rate squared (Equation (7)), this predicts an additional ~6 dB RIN enhancement for the less damped high slope efficiency VCSEL, which, together with the ~5 dB from the larger linewidth, brings the difference to ~11 dB in agreement with Fig. 7.

VI. CONCLUSION

While increasing the slope efficiency of a SM-VCSEL, and VCSELs in general, is effective for increasing the achievable output power, it results in an increase of both intensity and phase noise. The increased phase noise and linewidth is due to the higher spontaneous emission rate and lower photon density caused by the higher resonator loss. The increased RIN is additionally due to the less damped relaxation oscillations caused by the reduced photon lifetime.

The achievable output power from an oxide-confined SM-VCSEL is also dependent on the positioning of the oxide aperture with respect to the active region. The position controls the transverse current confinement and current spreading. In contrast to the dependence on slope efficiency, we find no noticeable dependence of either intensity or phase noise on current spreading for SM-VCSELs with similar suppression of higher order modes.

We show that 1060 nm oxide-confined SM-VCSELs with sufficiently low resonator loss have RIN approaching the shot noise level at high current and power (approximately -150 dB/Hz at 1 mW output power). More than 10 dB higher RIN levels are observed for the higher loss VCSELs.

Linewidths down to ~6 MHz and a linewidth-power product as low as 0.5 MHz·mW were measured for the low loss SM-VCSELs. The higher loss SM-VCSELs have more than three times higher linewidth-power products. Optical resonator and optical gain simulations were used to show that the small linewidth is a result of a small linewidth enhancement factor.

While GaAs-based oxide-confined VCSELs at 1060 nm were used in all measurements, the conclusions regarding the dependence of noise on resonator loss should be applicable to any SM-VCSEL, irrespective of material system and wavelength. The conclusions regarding current spreading should be applicable to oxide-confined VCSELs at any wavelength.

REFERENCES

[1] J. A. Tatum, D. Gazula, L. A. Graham, J. K. Guenter, R. H. Johnson, J. King, C. Kocot, G.D. Landry, I. Lyubomirsky, A. N. MacInnes, E. M. Shaw, K. Balemarthy, R. Shubochkin, D. Vaidya, M. Yan, and F. Tang, "VCSEL-based interconnects for current and future data centers," *IEEE J. Lightwave Technol.*, vol. 33, no. 4, pp. 727-732, Feb. 2015.

[2] J. F. Seurin, D. Zhou, G. Xu, A. Miglo, D. Li, T. Chen, B. Guo, and C. Ghosh, "High-efficiency VCSEL arrays for illumination and sensing in consumer applications," *Proc. SPIE*, vol. 9766, pp. 97660D 1-9, Mar. 2016.

[3] M. E. Warren, D. Podva, P. Dacha, M. K. Block, C. J. Helms, and J. Maynard, "Low-divergence high-power VCSEL arrays for Lidar application," *Proc. SPIE*, vol. 10552, pp. 105520E 1-10, Feb. 2018.

[4] E. Simpanen, J. S. Gustavsson, A. Larsson, M. Karlsson, W. V. Sorin, S. Mathai, M. R. Tan, and S. R. Bickham, "1060 nm single-mode VCSEL and single-mode fiber links for long-reach optical interconnects," *J. Lightwave Techn.*, vol. 37, no. 13, pp. 2963-2969, Jul. 2019.

[5] H. P. Zappe, F. Monti di Sopra, H. P. Gauggel, K. H. Gulden, R. Hövel, and M. Moser, "High-spectral purity VCSELs for spectroscopy and sensors," *Proc. SPIE*, vol. 3945, pp. 106-116, Mar. 2000.

[6] M. Grabherr, "VCSELs for optical mice and sensing," in VCSELs – fundamentals, technology and applications of vertical-cavity surface-emitting lasers, *Springer Series in Optical Sciences*, vol. 166, pp. 521-538, 2013.

[7] D. K. Serkland, G. M. Peakea, K. M. Geiba, R. Lutwakb, R. M. Garvey, M. Varghesec, and M. Mescherc, "VCSELs for atomic clocks," *Proc. SPIE*, vol. 6132, pp. 613208 1-11, Feb. 2006.

[8] L. G. Zei, S. Ebers, J. R. Kropp, and K. Petermann, "Noise performance of multimode VCSELs," *J. Lightwave Techn.*, vol. 19, no. 6, pp. 884-892, Jun. 2001.

[9] F. M. di Sopra, H. P. Zappe, M. Moser, R. Hovel, H.-P. Gauggel, and K. Gulden, "Near-infrared vertical-cavity surface-emitting lasers with 3-MHz linewidth," *IEEE Photon. Techn. Lett.*, vol. 11, no. 12, pp. 1533-1535, Dec. 1999.
[10] S. Blokhin, M. Bobrov, A. Blokhin, A. Kuzmenkov, A. Vasil'ev, Y. Zadiranov, E. Evropeytsev, A. Sakharov, N. Ledentsov, L. Karachinsky, A. Ospennikov, N. Maleev, and V. Ustinov, "Emission-line width and α-factor of 850-nm single-mode vertical-cavity surface-emitting lasers based on InGaAs/AlGaAs quantum wells," *Semiconductors*, vol. 52, no. 1, pp. 93-99, Jan. 2018.
[11] E. R. Hegblom, N. M. Margalit, B. Thibeault, L. A. Coldren, and J. E. Bowers, "Current spreading in apertured vertical-cavity lasers," *Proc. SPIE*, vol. 3003, pp. 176-180, Apr. 1997.
[12] E. Haglund, P. Westbergh, J. S. Gustavsson, E. P. Haglund, and A. Larsson, "High-speed VCSELs with strong confinement of optical fields and carriers," *IEEE J. Lightwave Technol.*, vol. 34, no. 2, pp. 269–277, Jan. 2016.
[13] J. Y. Law and G. P. Agrawal, "Noise properties of index-guided vertical-cavity surface-emitting lasers," *Proc. SPIE*, vol. 3625, pp. 404-413, Aug. 1999.
[14] K. M. van Vliet and H. Mehta, "Theory of transport noise in semiconductors," *Phys. Stat. Sol. B*, vol. 106, no. 11, pp. 11-30, Jul. 1981.
[15] A. Larsson, E. Simpanen, J. S. Gustavsson, E. Haglund, E. P. Haglund, T. Lengyel, P. A. Andrekson, W. V. Sorin, S. Mathai, M. Tan, and S. R. Bickham, "1060 nm VCSELs for long-reach optical interconnects," *Opt. Fiber Technol.*, vol. 44, pp. 36-42, Aug. 2018.
[16] P. Westbergh, J. S. Gustavsson, B. Kögel, Å. Haglund, and A. Larsson, "Impact of photon lifetime on high-speed VCSEL dynamics," *IEEE J. Sel. Top. Quantum El.*, vol. 17, no. 6, pp. 1603-1613, Nov./Dec. 2011.
[17] H. Li, P. Wolf, J. Lott, and D. Bimberg, "Relative intensity noise of temperature-stable, energy-efficient 980 nm VCSELs," *AIP Advances*, vol. 7, no. 2, 025107, Feb. 2017.
[18] J. Y. Law and G. P. Agrawal, "Effects of optical feedback on static and dynamic characteristics of vertical-cavity surface-emitting lasers," *IEEE J. Sel. Top. Quantum Electron.*, vol. 3, no. 2, pp. 353-358, Apr. 1997.
[19] A. L. Schawlow and C. H. Townes, "Infrared and optical masers," *Physical Rev.*, vol. 112, no. 6, pp. 1940-1949, Dec. 1958.
[20] C. H. Henry, "Theory of the linewidth of semiconductor lasers," *IEEE J. Quant. Electron.*, vol. 18, no. 2, pp. 259-264, Feb. 1982.
[21] L. A. Coldren, S. W. Corzine, and M. L. Masanovic, Diode Lasers and Photonic Integrated Circuits. Hoboken, New Jersey: Wiley, 2012.
[22] R. Michalzik and K. J. Ebeling, "Operating principles of VCSELs," in Vertical-Cavity Surface-Emitting Laser Devices, H. E. Li and K. Iga (eds.), *Springer Series in Photonics*, vol. 6., pp. 53-98, 2003.
[23] A. Tibaldi, F. Bertazzi, M. Goano, R. Michalzik, and P. Debernardi, "VENUS: a vertical-cavity surface-emitting laser electro-opto-thermal numerical simulator," *IEEE J. Sel. Top. Quantum Electron.*, vol. 25, no. 6, 1500212, Nov./Dec. 2019.
[24] R. Nagarajan and J. E. Bowers, "High-speed lasers," in Semiconductor Lasers II, E. Kapon (ed.), Academic Press Series in Optics and Photonics. San Diego: Academic Press, 1999.

Ewa Simpanen (M'16) received the B.Sc. 2013 and M.Sc. 2015 in electrical engineering, and the Ph.D. degree 2020 in Microtechnology and Nanoscience, from Chalmers University of Technology, Gothenburg, Sweden.

Her research is focused on longer wavelength GaAs-based VCSELs for extended-reach optical interconnects and her interests include semiconductor device fabrication and electrical and optical characterization. In 2017 she received an IPC Best Student Paper Award.

Johan S. Gustavsson received the M.Sc. degree in electrical engineering and the Ph.D. degree in photonics from the Chalmers University of Technology, Gothenburg, Sweden, in 1998 and 2003, respectively.

Since 2003, he has been a Researcher with the Photonics Laboratory, Department of Microtechnology and Nanoscience, Chalmers University of Technology, where he was an Assistant Professor from 2004 to 2008 and has been an Associate Professor since 2011. In 2009, he was a Visiting Scientist with CNR Polytechnico, Turin, Italy. He is currently working on 56-Gb/s 850-nm VCSELs for next generation datacom links, blue/green GaN VCSELs, high contrast gratings as feedback elements in microcavity lasers, and heterogeneous integration of III/V-based VCSEL material on Si-platform. He has authored or co-authored more than 140 scientific journal and conference papers. His research has been focused on semiconductor lasers for short to medium reach communication and sensing applications. This has included surface relief techniques for mode and polarization control in VCSELs, 1.3-μm InGaAs VCSELs/GaInNAs ridge waveguide lasers for access networks, 2.3–3.5-μm GaSb VCSELs for CO, CO2, and NH3 sensing, and tunable VCSELs via moveable mirror for reconfigurable optical interconnects. His current research interests include mode dynamics and noise in vertical-cavity surface-emitting lasers (VCSELs).

Pierluigi Debernardi was born in Casale Monferrato and received the Degree in electronics engineering from Politecnico di Torino, Turin, Italy, in 1987. Since 1989, he has been with the Italian National Council of Research at Politecnico di Torino. He is currently involved in modeling and designing VCSEL structures with noncircular and/or complex geometries, so as to achieve specific performances. His research interests include the field of the modeling of semiconductor materials and devices for optoelectronic applications.

Wayne V. Sorin (S'78-M'80-SM'98-F'01) received his Ph. D. in Electrical Engineering from Stanford University in 1986. After graduation he worked for over 14 years as a scientist in the area of fiber optics at Hewlett-Packard/Agilent Laboratories. He then spent 7 years at the start-up company Novera Optics. Later he spent a year at the University of Melbourne as a Senior Research Fellow. He currently working at Hewlett Packard Enterprise Labs in the area of short reach, high bandwidth computer communications.

Wayne is an inventor on over 136 US patents and an author on over 100 journal and conference papers. He was a contributing author for the textbook "Fiber Optic Test and Measurement" (Prentice Hall, 1997) and has also spent 4 years on the part-time faculty of San Jose State University. Wayne has been an Associate Editor for the IEEE journal "Photonics Technology Letters" and has served a 3-year term on the Board of Governors for the IEEE Lasers and Electro-Optics Society (LEOS). He was also the General Co-Chair for OFC'2002 (Optical Fiber Communications conference).

Sagi Mathai (S'97-SM'10) received the B.S., M.S. and Ph.D degrees in Electrical Engineering from the University of California, Los Angeles, in 1997, 2001, and 2004, respectively. From 2005 to 2007, he was a postdoctoral researcher at the University of California, Berkeley, where he worked on CMOS compatible MEMS tunable SOI microring optical modulators. He joined HP Labs in 2007 where he developed multi-drop optical backplanes and wafer scale packaging of 2D optical engines. He is currently a Principle Research Scientist in the Systems Architecture Lab at Hewlett Packard Laboratories investigating optoelectronic devices and transceivers, co-packaging, and optical interconnects for high performance computing and datacenters. He has authored or co-authored 62 technical publications, contributed 1 book chapter, and is an inventor on 60 issued patents. Sagi is a member of the IEEE Photonics, Microwave Theory and Techniques and Electronics Packaging Societies.

Michael R. Tan (M'84) received the Ph.D. degree in electrical engineering from Stanford University, Stanford, CA, USA, in 1984. He is currently a Distinguished Technologist in Hewlett-Packard Laboratories, Palo Alto, CA, USA, and leads a group focused on cost effective, high-bandwidth density photonic interconnects. His previous work focused on SAW, mm-wave and various optoelectronic devices used in both instrumentation and optical communications products. He is the coauthor of more than 80 journal articles and holds more than 90 patents.

Anders Larsson received the M.Sc. and Ph.D. degrees in electrical engineering from Chalmers University of Technology, Göteborg, Sweden, in 1982 and 1987, respectively. In 1991, he joined the faculty at Chalmers where he was promoted to Professor in 1994. From 1984 to 1985 he was with the Department of Applied Physics, California Institute of Technology, and from 1988 to 1991 with the Jet Propulsion Laboratory, both at Pasadena, CA, USA. He has been a guest professor at Ulm University (Germany), at the Optical Science Center, University of Arizona at Tucson (USA), at Osaka University (Japan), and at the Institute of Semiconductors, Chinese Academy of Sciences (China). He co-organized the IEEE Semiconductor Laser Workshop 2004, organized the European Semiconductor Laser Workshop 2004, was a co-program chair for the European Conference on Optical Communication 2004, and was the program and general chair for the IEEE International Semiconductor Laser Conference in 2006 and 2008, respectively. He was a member of the IEEE Photonics Society Board of Governors (2014-2016) and an associate editor for IEEE/OSA Journal of Lightwave Technology (2011-2016) and is a member of the editorial board of IET Optoelectronics. His scientific background is in the areas of optoelectronic materials and devices for optical communication, information processing, and sensing. Currently, his research is focused on vertical cavity surface emitting lasers and optical interconnects. He has published more than 500 scientific journal and conference papers and 2 book chapters. He is a Fellow of IEEE, OSA, and EOS. In 2012 he received the HP Labs Research Innovation Award.